2024 IEEE/RSJ International Conference on Intelligent Robots and Systems (IROS)
October 14-18, 2024. Abu Dhabi, UAE

A Laser-Induced Graphene-Based Flexible Multimodal Sensor for Material and Texture Perception

Youning Duo, Jinxi Duan, Xingyu Chen, Wenbo Liu, Shengxue Wang, and Li Wen

***Abstract*— Humans can perceive and interact with their surroundings through multiple senses. For intelligent robots, multimodal sensors are crucial for them to perceive and understand the environment. In this work, we propose a multi-layered flexible multimodal sensor based on laser-induced graphene, capable of detecting both touchless signals (such as the distance from external objects and their material) and tactile signals (three-dimensional force). The sensor has advantages in durability and stability. Under normal force, the sensitivity is –7.449% N^{-1} in the range of 0 N to 1.5 N and –0.273% N^{-1} in the range of 1.5 N to 30 N, with fast response (17 ms) and recovery (37 ms). Furthermore, using the Convolutional Neural Networks (CNN) model, we develop an intelligent soft robot system capable of distinguishing objects of different materials and fabric textures with accuracies of 99% and 88.75%, respectively. The proposed flexible multimodal sensor holds a significant effect on the perception and interaction of intelligent robots with the environment.**

I. Introduction

In the last few years, flexible sensors have attracted great attention and have been under intensive investigation for their remarkable applications in areas including health monitoring [1], prosthetics [2], and robotics [3]. Based on sensing principles, flexible sensors can be categorized into capacitance [4], resistance [5], triboelectric nanogenerator (TENG) [6], piezoelectric [7], magnetism [8], and optical [9]. Flexible multimodal sensors, further on, can simultaneously detect two or more kinds of signals such as strain, pressure, temperature, humidity, etc. [10], [11], [12], [13], enabling the perception of richer environmental information at the same time. Similar to the human body, which utilizes multiple senses to gather diverse information from the surroundings, aiding in human-environment interaction [14], multimodal sensors play a crucial role for robots in exploring and understanding the environment, facilitating decision-making in robotic control systems [15], [16]. Among these, the acquisition of touchless and three-dimensional force signals is particularly essential for robots. Touchless information helps robots assess the distance from objects and rapidly gather features of objects such as shape and material without physical contact [17]. Three-dimensional force information is beneficial for robots to perceive the surface characteristics of objects and manipulate objects dexterously [18]. Additionally, with the rapid development of artificial intelligence, various intelligent sensor systems combined with machine learning algorithms have emerged [19], [20]. However, it remains a significant challenge to develop a robust, low-cost, and highly integrated flexible multimodal sensor [21], [22].

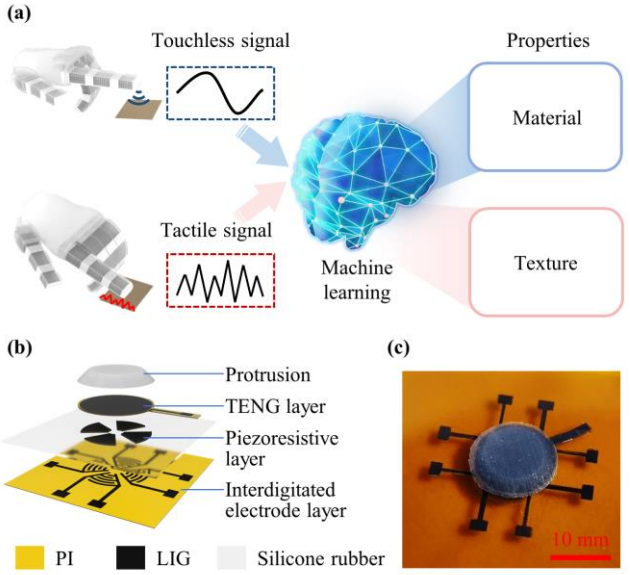

Figure 1. Overview of the robotic system and the flexible multimodal sensor. (a) A robotic sensory system for material and texture perception. (b) Structure of the flexible multimodal sensor. (c) Physical image of the flexible multimodal sensor.

In the past decade, laser-induced graphene (LIG) has experienced rapid development and has been widely applied in electronic skin [23], flexible heater [24], supercapacitor [25], and other fields. Laser-induced graphene is typically generated by irradiating synthesized polymer materials (such as polyimide (PI)) with CO_2 infrared laser [26]. This method allows for the rapid, mask-free, and cost-effective processing of graphene patterns with excellent electrical performance and high stability. Computer-controlled infrared lasers facilitate convenient adjustment of laser processing parameters, enabling the fabrication of patterned electrodes with varying electrical properties, mechanical properties, and microstructures [27]. Flexible sensors based on laser-induced graphene have the capability to detect various physical signals [28] and chemical signals [29]. Thus, it is a reliable strategy to engineer the flexible multimodal sensor via laser-induced graphene.

In this study, we designed a flexible multimodal sensor based on laser-induced graphene, capable of detecting touchless signals and tactile signals (differentiation of three-dimensional forces). We successfully fabricated laser-induced graphene electrodes with different features by

*This work was supported by the National Key R&D Program of China (Grant Nos. 2022YFB4701800), and the National Science Foundation support projects, China (Grant Nos. T2121003, 92048302, 62425303).

Youning Duo, Jinxi Duan, Xingyu Chen, Shengxue Wang and Li Wen are with the School of Mechanical Engineering and Automation, Beihang University, Beijing 100191, China. E-mail: liwen@buaa.edu.cn.

Wenbo Liu is with the School of Aerospace Engineering, Tsinghua University, Beijing 100084, China.

controlling the laser's parameter, thereby achieving the production of functional layers with different properties. It exhibits characteristics of sensitivity, stability, and rapid response. Utilizing Convolutional Neural Networks (CNN), as illustrated in Fig. 1(a), we established an intelligent soft robot system. The flexible multimodal sensor enabled the soft robotic hand to detect multimodal information, such as identifying objects with different materials and fabrics with different textures, achieving accuracies of 99% and 88.75%, respectively. The proposed flexible multimodal sensor holds a significant effect on the perception and interaction of intelligent robots with the environment.

The rest of the paper is organized as follows: Section II presents the design and fabrication process of the flexible multimodal sensor, Section III describes the experiments and results of the sensing performance and the intelligent robot system, and Section IV concludes the paper.

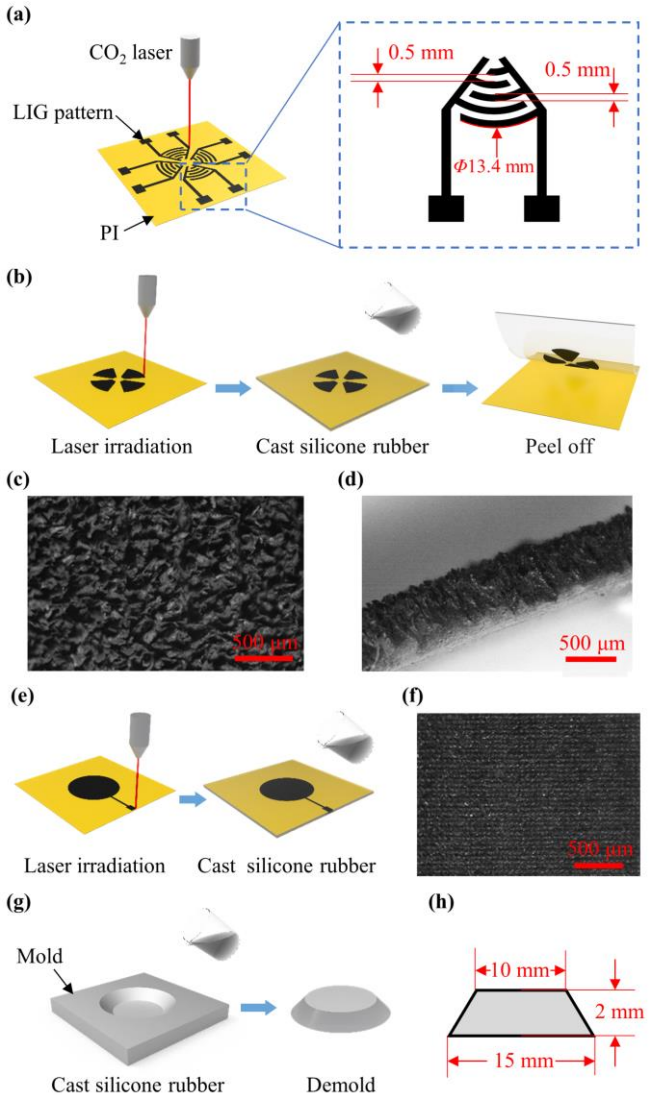

Figure 2. Fabrication process of the flexible multimodal sensor. (a) Preparation process of the interdigitated electrode. (b) Preparation process of the piezoresistive layer. (c) Optical microscopic image of the porous graphene structure. (d) Cross-sectional optical microscopic image of the transferred porous piezoresistive unit. (e) Preparation process of the TENG layer. (f) Optical microscope image of the TENG graphene electrode. (g) Preparation process of the protrusion. (h) The size of the protrusion.

II. Design and Fabrication

A. Structure of the flexible multimodal sensor

The overall structure of the flexible multimodal sensor is shown in Fig. 1(b). From top to bottom, the flexible multimodal sensor is composed of a protrusion, a TENG layer, a piezoresistive layer, and an interdigitated electrode layer. Specifically, the electrodes of the TENG layer, piezoresistive layer, and interdigitated electrode layer were all fabricated with laser-induced graphene. A physical image of the flexible multimodal sensor is depicted in Fig. 1(c).

B. Preparation process of the interdigitated electrode layer

We utilized a 10.6 μm CO_2 infrared laser engraving machine (VLS 2.30, Universal Laser Systems) to irradiate PI film (0.1 mm thick, Hongxin), and patterned graphene interdigitated electrodes were made directly on the PI substrate as shown in Fig. 2(a). The scanning power, image density, and scan speed were set as 2.1 W, 500 PPI, and 127 mm/s, respectively. The diameter of the interdigitated electrodes' outer ring was 13.4 mm. The minimum line width and line spacing were 0.5 mm.

C. Preparation process of the piezoresistive layer

The fabrication process of the piezoresistive layer is illustrated in Fig. 2(b). First, 0.1 mm thick PI film was irradiated by CO_2 infrared laser, creating porous graphene units on the PI substrate. The scanning power, image density, and scan speed were set as 6 W, 500 PPI, and 101.6 mm/s, respectively. Subsequently, a layer of silicone rubber (Dragon Skin 20, Smooth-On) was cast on the substrate. After curing for 1 hour at 90 °C, it was peeled off. This process transferred the porous graphene structure from the PI film onto the silicone rubber. The optical microscopic image of the fabricated porous graphene structure is shown in Fig. 2(c), while Fig. 2(d) displays the cross-sectional optical microscopic image of the transferred porous piezoresistive unit. The four units of the piezoresistive layer correspond to the four interdigitated electrodes. The piezoresistive layer was then placed above the interdigitated electrode layer and bonded together using silicone adhesive (Sil-Poxy, Smooth-on).

D. Preparation process of the TENG layer

The processing flow of the TENG layer is shown in Fig. 2(e). Firstly, 0.1 mm thick PI film was irradiated by CO_2 infrared laser, and a patterned graphene electrode was made on the PI substrate. The diameter of the circular electrode was 13.4 mm. The scanning power, image density, and scan speed were set as 2.1 W, 500 PPI, and 127 mm/s, respectively. Then a layer of silicone rubber (Dragon skin 20, Smooth-on) was spin-coated on the PI film as a dielectric layer and cured at 90 °C for 1 hour. The optical microscope image of the TENG graphene electrode is shown in Fig. 2(f). Compared with the piezoresistive layer, the graphene electrode microstructure of the TENG layer is flatter. The TENG layer is combined with the piezoresistive layer by silicone adhesive (Sil-Poxy, Smooth-on).

E. Preparation process of the protrusion

As shown in Fig. 2(g), silicone rubber (Dragon skin 20, Smooth-on) was cast in a 3D printed photosensitive resin mold, and then removed after curing at room temperature for 4

hours. The protrusion is in the shape of a cone frustum, and its size is shown in Fig. 2(h). The height, upper surface circular diameter, and lower surface circular diameter of the cone frustum were 2 mm, 10 mm, and 15 mm, respectively. The protrusion's lower surface was connected with the TENG layer through silicone adhesive (Sil-Poxy, Smooth-on).

III. Experiments and Results

A. Performance of touchless sensing

The touchless sensing function of the flexible multimodal sensor relies on the TENG layer, and the sensing principle of touchless sensing is shown in Fig. 3(a). Based on the triboelectric effect, due to the varying electron binding capabilities of different materials, after an external object continuously contacts with and separates from the sensor, the surfaces of both the object and the sensor acquire equal but opposite charges, as illustrated in state (i). As shown in state (ii), when the charged external object gradually approaches the sensor, the electric potential of the TENG electrode will change based on the principle of the electrostatic induction effect. We placed a 4×4 cm^2 acrylic plate at the end of a linear motor (E1100, LinMot) and controlled the distance between the acrylic plate and the sensor via the linear motor. The acrylic plate started to move toward the sensor at 30 mm away from the sensor's upper surface. In this process, the touchless signal was collected by using an electrometer (6514, Keithley) and a data acquisition card (USB-6356, National Instruments) with a sampling rate of 1000 Hz. The relationship between the touchless signal of the sensor and the distance from the acrylic plate to the sensor is shown in Fig. 3(b). As can be seen from the figure, when the distance to the sensor decreased during the movement of the acrylic plate, the output signal of the touchless sensing increased. Additionally, we verified the stability of the touchless sensing of the multimodal sensor. We controlled the linear motor to make the acrylic plate move cyclically over 400 times for 1000 seconds within the range of 0 mm to 30 mm from the sensor. The signal of the touchless sensing during this cyclic motion is shown in Fig. 3(c), demonstrating the excellent cyclic stability of the touchless sensing.

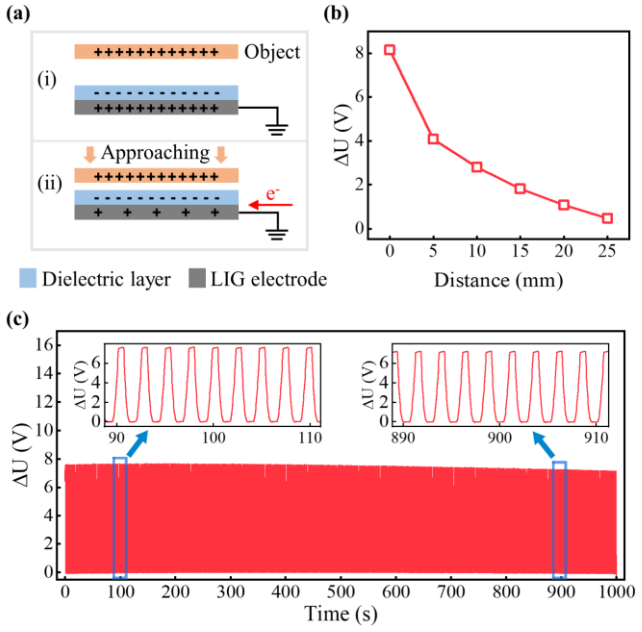

Figure 3. Characterization results of touchless sensing. (a) The principle of touchless sensing. (b) Touchless output signals were tested under different distances between the acrylic plate and the sensor. (c) Touchless output signals of the stability and durability test.

B. Performance of tactile sensing

There are four fan-shaped piezoresistive units on the piezoresistive layer. Each piezoresistive unit, in combination with its corresponding interdigitated electrode, forms a variable resistor tactile cell. Due to the porous structure of the piezoresistive units, external pressure causes the porous structure deformation, resulting in a decrease or increase in the resistance of the tactile cells. As depicted in Fig. 4(a), we constructed a platform for detecting normal force applied to the sensor. We utilized a linear motor (E1100, LinMot) to provide reciprocating motion and a force gauge (Mini 40, ATI Industrial Automation) to detect force. The flexible multimodal sensor was adhered to a glass sheet. Fig. 4(b) depicts a top view of the interdigitated electrode layer, with tactile cell numbers and coordinate axes as illustrated in the diagram. The z-axis is determined by the right-hand system. We established a voltage divider circuit and used a data acquisition card (USB-6356, National Instruments) to collect analog signals with a sampling rate of 1000 Hz. Fig. 4(c) displays the response performance of the sensor under a fast press, with the response and recovery time of the sensor tactile sensing recorded as 17 ms and 37 ms, respectively, indicating excellent response capabilities. As a normal force F_z was applied to the sensor, the relative change in resistance of the sensor is illustrated in Fig. 4(d), where ΔR denotes the change in resistance, and R_{ini} represents the initial resistance of the tactile cells. When the normal force F_z gradually increased from 0 N to 30 N, the resistance of the four cells all decreased. Because the four tactile cells experienced the same component forces in the z-direction, as shown by

$$F_{1z} = F_{2z} = F_{3z} = F_{4z} = \frac{1}{4}F_z, \tag{1}$$

where F_{iz} (i=1,2,3,4) denotes the force in the z-direction loaded on each tactile cell, we defined the overall response of the flexible multimodal sensor to the normal force as

$$R_z = \frac{1}{4}\left(\frac{\Delta R_1}{R_{1ini}} + \frac{\Delta R_2}{R_{2ini}} + \frac{\Delta R_3}{R_{3ini}} + \frac{\Delta R_4}{R_{4ini}}\right), \tag{2}$$

where ΔR_j (j=1,2,3,4) denotes the resistance change of each tactile cell and R_{jini} (j=1,2,3,4) denotes the initial resistance of each tactile cell. As shown in Fig. 4(e), R_z exhibits linear trends with the normal force in the ranges of 0 N to 1.5 N and 1.5 N to 30 N, and the sensitivity S (the ratio of the relative change of R_z to the normal force) is –7.449% N^{-1} and –0.273% N^{-1}, respectively. Additionally, we evaluated the stability of the tactile cells by cyclically applying a normal force of 10N using the linear motor over 400 times in 650 seconds. The resistance changes of the four tactile cells of the sensor, as shown in Fig. 4(f), demonstrate the excellent cyclic stability of the sensor's tactile cells.

We also tested the flexible multimodal sensor's ability to detect shear forces. We set up a shear force detection platform as shown in Fig. 5(a). The linear motor moved horizontally indicated by the red arrow, driving the 3D-printed model to

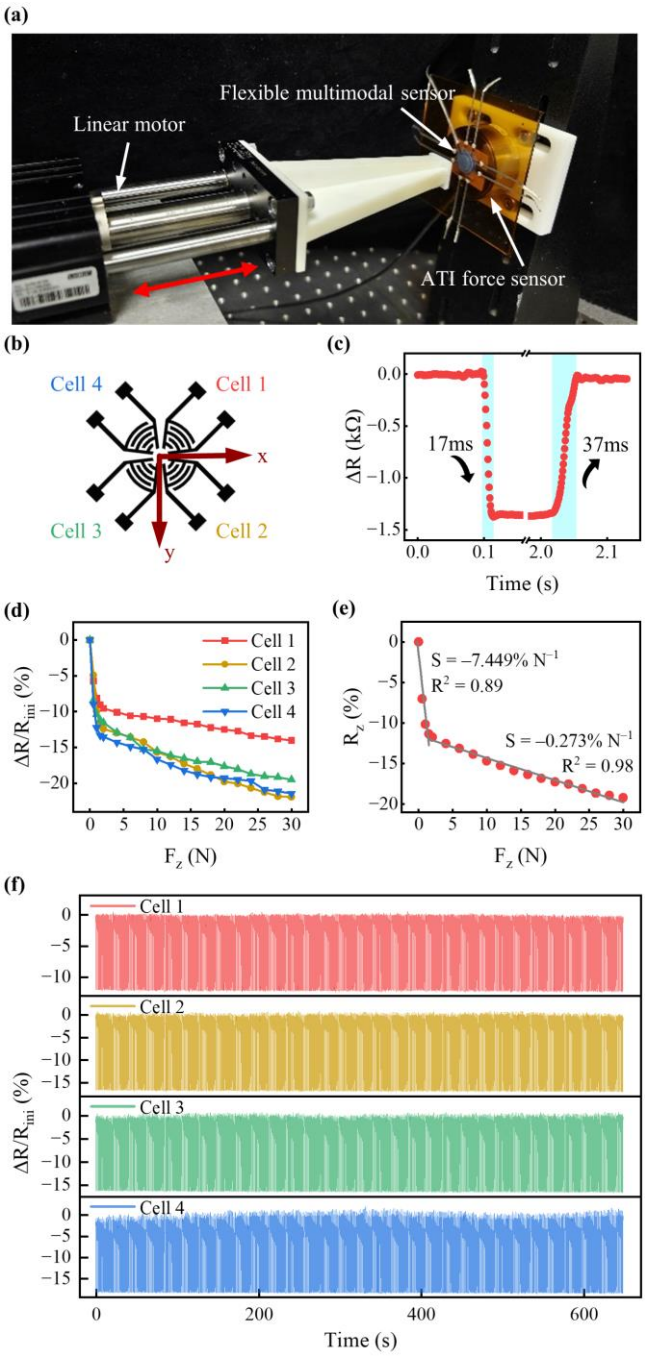

Figure 4. Characterization results of tactile sensing to normal force. (a) The experimental platform for testing normal force. (b) The cell numbers and coordinate axes. (c) The response and recovery process of the sensor under a fast press. (d) Tactile output signals were tested under different normal forces applied to the sensor. (e) The overall response of the flexible multimodal sensor to normal force. (f) Tactile output signals of the stability and durability test.

apply shear force to the sensor. The principle of the sensor to detect shear force is shown in Fig. 5(b). Under the action of shear force, the four tactile cells produce different deformation, resulting in different change trends in the resistance of them, so as to detect the shear force. Under 10 N normal force preload, we applied shear force to the sensor in the x-direction, as depicted in Fig. 5(c). Here, R represents the current resistance of the tactile cells, R_{10} denotes the resistance

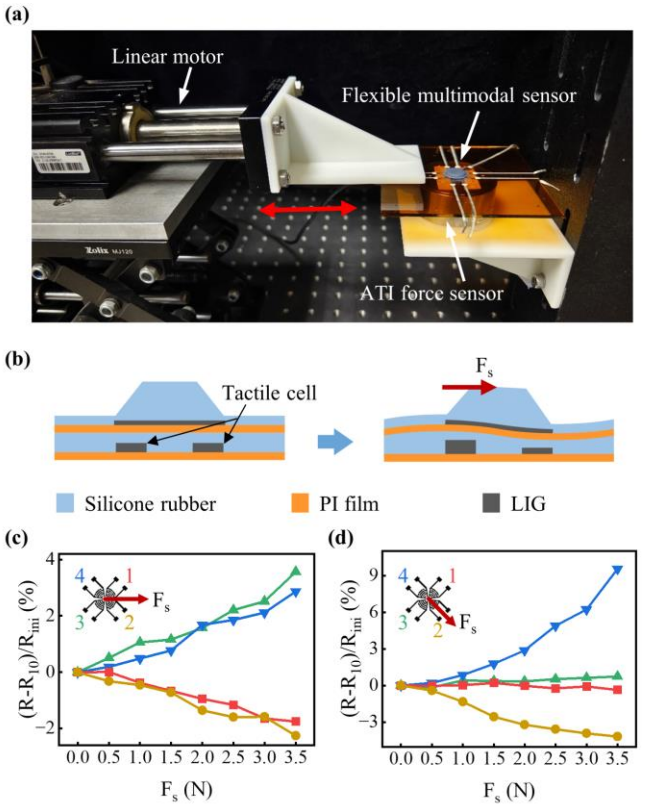

Figure 5. Characterization results of tactile sensing to shear force. (a) The experimental platform for testing shear force. (b) Schematic diagram of the principle of detecting shear force. (c) Tactile output signals were tested under different shear forces applied to the sensor toward the x-direction. (d) Tactile output signals were tested under different shear forces applied to the sensor toward cell 2.

value when applying a 10 N normal force preload, and R_{ini} is the resistance without any force. As the shear force gradually increased from 0 N to 3.5 N, the resistance of tactile cell 1 and cell 2 decreased, while the resistance of cell 3 and cell 4 increased. In Fig 5(d), we applied shear force towards tactile cell 2 under a 10 N normal force preload. As the shear force increased from 0 N to 3.5 N, the resistance of cell 2 decreased, the resistance of cell 4 increased, while the resistance of cell 1 and cell 3 remained almost unchanged. This demonstrates that the sensor can detect shear forces by observing the different resistance trends in the four tactile cells.

C. Multimodal perception with machine learning

In order to demonstrate the effectiveness of the flexible multimodal sensor in a robot system, we combined the flexible multimodal sensor with a bionic soft robotic hand, as shown in Fig 6(a). The soft robotic hand was made of silicone rubber (E610, Guoyuan), with a 3D-printed resin structure serving as a skeletal support in the center of the palm. The fingers can be actuated by air pressure. The flexible multimodal sensor was attached to the fingertip of the soft robotic hand, giving the robotic hand the ability of touchless and tactile perception. Based on the principle of the TENG sensor, this sensor can perceive the distance between external objects and the robotic hand in a non-contact manner. Moreover, due to the varying electrification characteristics of different materials, when objects approach the sensor from the same distance, the TENG

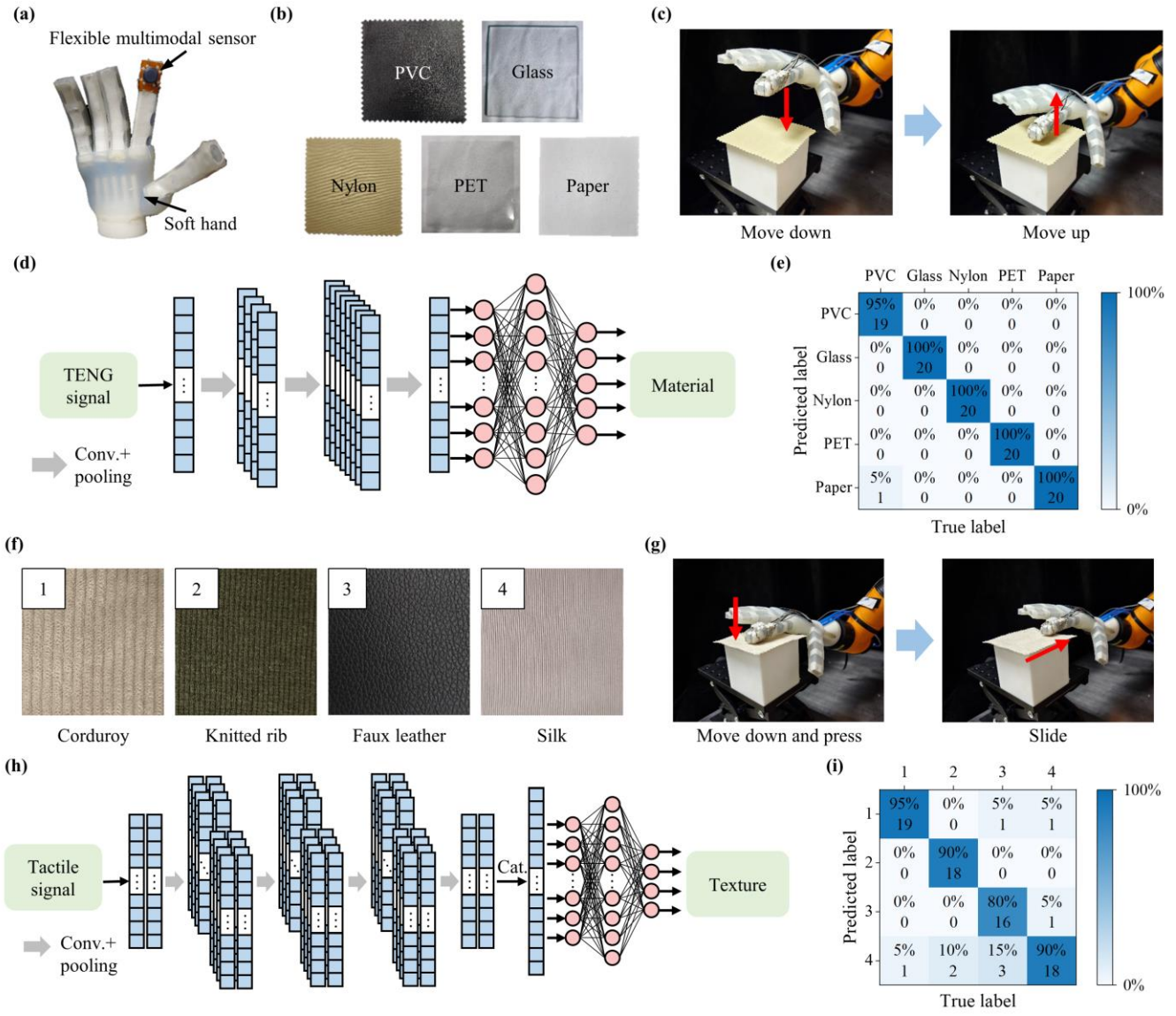

Figure 6. The intelligent soft robotic hand equipped with the flexible multimodal sensor could recognize the material and texture of objects. (a) The image of the soft robotic hand equipped with the flexible multimodal sensor. (b) The materials for recognition (PVC, glass, nylon, PET, and paper). (c) Schematic diagram of the soft robotic hand movement process. (d) The CNN model for material detection. (e) The confusion matrix for recognizing the material of objects (total accuracy: 99%). (f) The fabrics with different textures for recognition (in numerical order, they are corduroy, knitted rib, faux leather, and silk). (g) Schematic diagram of the soft robotic hand movement process when touching fabrics. (h) The CNN model for texture detection. (i) The confusion matrix for recognizing fabrics texture (total accuracy: 88.75%).

electrode detects signals with different amplitudes, which can be used to distinguish the material of the objects. As shown in Fig. 6(b), we selected five different materials (PVC, glass, nylon, PET, and paper). Subsequently, we mounted the soft robotic hand on a robotic arm (i5, AUBO Robotics). The soft robotic hand descended gradually toward the surface of the object from a starting height of 60 mm above and then moved back to the initial position at a speed of 0.1 m/s, as depicted in Fig. 6(c). We collected touchless signals from the TENG sensor during this process and used machine learning algorithms to identify different materials. The CNN model used here is shown in Fig 6(d). The CNN model for material recognition incorporates three convolutional layers, two pooling layers, two fully connected layers, and two ReLU (Rectified Linear Unit) activation layers, focusing on differentiating amplitude information within the signals. To train the material recognition model, we employed datasets from five distinct material objects, each contributing ten sets of data. The online recognition experiment is shown in the supplementary video, and 99% recognition accuracy can be achieved as shown in Fig. 6(e).

Additionally, we verified the tactile sensing capabilities of the flexible multimodal sensor. We selected four fabrics with different textures, as depicted in Fig. 6(f), namely corduroy, knitted rib, faux leather, and silk. Controlling the soft robotic hand to press onto the fabrics and slide backward indicated by the red arrow at a speed of 0.1 m/s, we collected the signals from the tactile sensing cells during this process, as shown in Fig. 6(g). We constructed a CNN model to distinguish fabric textures, as illustrated in Fig. 6(h). The texture recognition CNN model comprises four convolutional layers, three pooling layers, two fully connected layers, and two ReLU

activation layers, enabling the identification of signal features such as frequency fluctuations and amplitude variations. The texture recognition model was trained using datasets from four different objects, each contributing fifteen data sets to the training dataset. The online recognition experiment is shown in the supplementary video, and our intelligent soft robotic hand system achieved recognition accuracy of 88.75% as shown in Fig. 6(i).

IV. Conclusion and Discussion

In this study, we designed a flexible multimodal sensor based on laser-induced graphene. The sensor features a layered structure, enabling detection of touchless signals (such as the distance from external objects and the material of objects) and differentiation of three-dimensional forces. It possesses characteristics of sensitivity, stability, and fast response. The sensitivity to normal force is –7.449% N^{-1} in the range of 0 N to 1.5 N and –0.273% N^{-1} in the range of 1.5 N to 30 N. The response and recovery time to normal force is 17 ms and 37 ms, respectively. Utilizing Convolutional Neural Network, we constructed an intelligent soft robotic hand system capable of recognizing and distinguishing different materials and textures with accuracies of 99% and 88.75%, respectively. We verified that the flexible multimodal sensor can play an important role in the robot system. The proposed flexible multimodal sensor holds significant importance for intelligent robot perception and interaction with the environment. While our sensor has achieved preliminary success in multimodal detection, there are still some limitations. We only implemented the initial integration of the flexible multimodal sensor with a soft robotic hand. Exploring deeper integration with robots, such as incorporating sensor signals into the robot's closed-loop control system and utilizing the flexible multimodal sensor to assist the soft robotic hand in exploring and interacting with the environment, is worth further investigation.

In future work, we will continue to optimize the sensor's performance. Optimizing manufacturing processes to achieve large-area, high-density sensor production, and enabling the acquisition of extensive, multimodal information remains a challenge. Moreover, we will explore advanced integration methods of the flexible multimodal sensor with intelligent robotic systems (such as those based on large language models) to further enhance the role of flexible multimodal sensors in robotic systems.

References

[1] H. U. Chung et al., "Binodal, wireless epidermal electronic systems with in-sensor analytics for neonatal intensive care," Science, vol. 363, no. 6430, p. eaau0780, Mar. 2019.

[2] A. Chortos, J. Liu, and Z. Bao, "Pursuing prosthetic electronic skin," Nature Mater, vol. 15, no. 9, pp. 937–950, Sep. 2016.

[3] W. Liu et al., "Touchless interactive teaching of soft robots through flexible bimodal sensory interfaces," Nat Commun, vol. 13, no. 1, p. 5030, Aug. 2022.

[4] C. M. Boutry et al., "A hierarchically patterned, bioinspired e-skin able to detect the direction of applied pressure for robotics," Sci. Robot., vol. 3, no. 24, p. eaau6914, Nov. 2018.

[5] J. Ji, W. Zhao, Y. Wang, Q. Li, and G. Wang, "Templated laser-induced-graphene-based tactile sensors enable wearable health monitoring and texture recognition via deep neural network," ACS Nano, vol. 17, no. 20, pp. 20153–20166, Oct. 2023.

[6] Z. H. Guo et al., "Bioinspired soft electroreceptors for artificial precontact somatosensation," Sci. Adv., vol. 8, no. 21, p. eabo5201, May 2022.

[7] J. Zhang et al., "Finger-inspired rigid-soft hybrid tactile sensor with superior sensitivity at high frequency," Nat Commun, vol. 13, no. 1, p. 5076, Aug. 2022.

[8] H. Hu et al., "Wireless flexible magnetic tactile sensor with super-resolution in large-areas," ACS Nano, vol. 16, no. 11, pp. 19271–19280, Nov. 2022.

[9] H. Zhao, K. O'Brien, S. Li, and R. F. Shepherd, "Optoelectronically innervated soft prosthetic hand via stretchable optical waveguides," Sci. Robot., vol. 1, no. 1, p. eaai7529, Dec. 2016.

[10] J. Ge et al., "A bimodal soft electronic skin for tactile and touchless interaction in real time," Nat Commun, vol. 10, no. 1, p. 4405, Dec. 2019.

[11] H. L. Wang et al., "A dual‐responsive artificial skin for tactile and touchless interfaces," Small, vol. 19, no. 21, p. 2206830, May 2023.

[12] M. Liu et al., "A star-nose-like tactile-olfactory bionic sensing array for robust object recognition in non-visual environments," Nat Commun, vol. 13, no. 1, p. 79, Jan. 2022.

[13] J. Zhu et al., "A heterogeneously integrated spiking neuron array for multimode‐fused perception and object classification," Advanced Materials, vol. 34, no. 24, p. 2200481, Jun. 2022.

[14] M. O. Ernst and M. S. Banks, "Humans integrate visual and haptic information in a statistically optimal fashion," Nature, vol. 415, no. 6870, pp. 429–433, Jan. 2002.

[15] S. E. Navarro et al., "Proximity perception in human-centered robotics: A survey on sensing systems and applications," IEEE Trans. Robot., vol. 38, no. 3, pp. 1599–1620, Jun. 2022.

[16] B. Wu, T. Jiang, Z. Yu, Q. Zhou, J. Jiao, and M. L. Jin, "Proximity sensing electronic skin: Principles, characteristics, and applications," Advanced Science, p. 2308560, Jan. 2024.

[17] W. Liu et al., "An intelligent robotic system capable of sensing and describing objects based on bimodal, self-powered flexible sensors," Adv Funct Materials, vol. 33, no. 41, p. 2306368, Oct. 2023.

[18] H. Yu et al., "Skin‐inspired capacitive flexible tactile sensor with an asymmetric structure for detecting directional shear forces," Advanced Science, p. 2305883, Dec. 2023.

[19] G. Li, S. Liu, L. Wang, and R. Zhu, "Skin-inspired quadruple tactile sensors integrated on a robot hand enable object recognition," Sci. Robot., vol. 5, no. 49, p. eabc8134, Dec. 2020.

[20] K. Tao et al., "Deep-learning enabled active biomimetic multifunctional hydrogel electronic skin," ACS Nano, p. acsnano.3c05253, Jul. 2023.

[21] Y. Luo et al., "Technology roadmap for flexible sensors," ACS Nano, vol. 17, no. 6, pp. 5211–5295, Mar. 2023.

[22] K. Xu, Y. Lu, and K. Takei, "Multifunctional skin-inspired flexible sensor systems for wearable electronics," Adv Materials Technologies, vol. 4, no. 3, p. 1800628, Mar. 2019.

[23] H. Wang, Z. Zhao, P. Liu, and X. Guo, "Laser-induced graphene based flexible electronic devices," Biosensors, vol. 12, no. 2, p. 55, Jan. 2022.

[24] I. Naseri, M. Ziaee, Z. N. Nilsson, D. R. Lustig, and M. Yourdkhani, "Electrothermal performance of heaters based on laser-induced graphene on aramid fabric," ACS Omega, vol. 7, no. 4, pp. 3746–3757, Feb. 2022.

[25] M. R. R. Abdul-Aziz et al., "High performance supercapacitor based on laser induced graphene for wearable devices," IEEE Access, vol. 8, pp. 200573–200580, 2020.

[26] Y. Xu et al., "Laser-induced graphene for bioelectronics and soft actuators," Nano Res., vol. 14, no. 9, pp. 3033–3050, Sep. 2021.

[27] T. D. Le et al., "Recent advances in laser‐induced graphene: mechanism, fabrication, properties, and applications in flexible electronics," Adv Funct Materials, vol. 32, no. 48, p. 2205158, Nov. 2022.

[28] H. Wang, Z. Zhao, P. Liu, and X. Guo, "A soft and stretchable electronics using laser-induced graphene on polyimide/PDMS composite substrate," npj Flex Electron, vol. 6, no. 1, p. 26, Apr. 2022.

[29] R. Wang et al., "Recent progress in high-resolution tactile sensor array: From sensor fabrication to advanced applications," Progress in Natural Science: Materials International, vol. 33, no. 1, pp. 55–66, Feb. 2023.